



Effect of the support on the hydrodeoxygenation of *m*-cresol over molybdenum oxide based catalysts

Vinicius O.O. Gonçalves^a, Carmen Ciotonea^b, Sandrine Arrii-Clacens^a, Nadia Guignard^a, Christelle Roudaut^a, Julie Rousseau^a, Jean-Marc Clacens^a, Sébastien Royer^b, Frédéric Richard^{a,*}

^a Institut de Chimie des Milieux et Matériaux de Poitiers, UMR 7285 Université de Poitiers—CNRS, 4, rue Michel Brunet, BP633, 86022 Poitiers Cedex, France
^b Univ. Lille, CNRS, ENSCL, Centrale Lille, Univ. Artois, UMR 8181—UCCS—Unité de Catalyse et de Chimie du Solide, F-59000 Lille, France

ARTICLE INFO

Article history:

Received 24 February 2017
 Received in revised form 24 April 2017
 Accepted 2 May 2017
 Available online 4 May 2017

Keywords:

m-Cresol
 HDO
 $\text{MoO}_x/\text{SBA-15}$
 $\text{MoO}_x/\text{SiO}_2$
 $\text{MoO}_x/\text{Al}_2\text{O}_3$

ABSTRACT

The hydrodeoxygenation (HDO) of *m*-cresol was investigated over supported molybdenum oxide catalysts at 340 °C under 4 MPa as total pressure. All catalysts were fully characterized using several techniques such as atomic absorption, N₂ physisorption, XRD, H₂-TPR, NH₃-TPD, Raman spectroscopy, TEM analysis and oxygen chemisorption. It was noted that the reducibility of molybdenum species depends on the support used and follows the same order than the one determined from the HDO activity, i.e. $\text{MoO}_x/\text{Al}_2\text{O}_3 > \text{MoO}_x/\text{SBA-15} > \text{MoO}_x/\text{SiO}_2$. In addition, the use of an ordered mesoporous silica support (SBA-5) or an acidic support (Al₂O₃) favored significantly the dispersion of MoO_x particles compared to SiO₂.

Under these experimental conditions, *m*-cresol transformation underwent through two parallel deoxygenation routes which involved either the direct C—O bond scission leading to toluene (DDO route), or the total hydrogenation of the aromatic ring yielding mainly to a mixture of methylcyclohexene isomers (HYD route). Regardless of the support used, the DDO route was always predominant. A reaction mechanism was proposed to explain the formation of toluene, the main product observed from HDO of *m*-cresol. To explain the formation of this aromatic, a selective adsorption through the oxygen atom of the phenolic reactant on oxygen vacancies, acting as HDO active sites, was proposed.

© 2017 Elsevier B.V. All rights reserved.

1. Introduction

The phenolic fraction issued from biomass pyrolysis has attracted attention due to its potential as a source of several biosourced products such as resins, carbon fibers, biofuels, additives, and aromatic chemicals (Benzene, Toluene and Xylene or BTX) [1–3]. Regarding the composition of biomass, an important part is constituted of lignin which is the most widely available renewable source of aromatics [4]. Nowadays, the majority of the bulk BTX are produced from fossil resources, mostly by the catalytic reforming of naphtha in a petroleum refinery, which is tied to the traditional petro-based platform [5]. The replacement of the fossil resources by biosourced raw materials has been continuously developed in biorefineries [6].

Hydrodeoxygenation (HDO) process is a promising technology to produce value-added products from oxygenated compounds. This process allows to upgrade the phenolic pyrolysis fraction through the elimination of oxygen atoms as water and/or carbon oxides (CO and CO₂). In this process, aromatic oxygenates are exposed to a H₂ atmosphere, at temperatures between 250 and 500 °C, in the presence of a solid catalyst [7,8]. It is noteworthy that to produce aromatics from phenolic compounds, it is a requirement during HDO to remove oxygen atoms while limiting the hydrogen consumption [9].

Many efforts have been made to design efficient catalyst formulations for the hydrotreatment of oxygenated compounds. Sulfided Mo-based catalysts were first studied for the HDO reactions since they were already used in hydrotreatment processes implemented in conventional oil refineries to decrease the sulfur content from petroleum [10]. Their uses for the treatment of bio-oils from biomass is rather not preferable due to environmental concerns relative to the possible contamination of HDO products by sulfur [11,12].

* Corresponding author.

E-mail address: frédéric.richard@univ-poitiers.fr (F. Richard).



Recently, molybdenum oxide (MoO_x) was evaluated as catalyst for the HDO of both model molecules [9,13–15] and pyrolysis bio-oils [16,17]. Interestingly, molybdenum oxide, which can be considered as an environment-friendly and also a cost-effective material, showed the highest activity in HDO among a series of metal oxides (MoO_3 , V_2O_5 , Fe_2O_3 , CuO and WO_3) [9]. At 320 °C under atmospheric pressure, Shetty et al. [14] reported that several supported MoO_x catalysts ($\text{MoO}_x/\text{SiO}_2$, $\text{MoO}_x/\text{Al}_2\text{O}_3$, $\text{MoO}_x/\text{TiO}_2$ and $\text{MoO}_x/\text{ZrO}_2$) can selectively cleave the C–O bond of *m*-cresol without hydrogenate the aromatic ring. Toluene was obtained at high selectivities, from 76 and 99 mol%. The authors proposed that the catalytic activity was dependent on the reducibility of Mo species but also on the electronegativity of the support cation. Prasomsri and co-workers [9,13] only observed aromatic production (mainly benzene and toluene) during the HDO of anisole over unsupported MoO_3 catalyst, under similar experimental conditions (320–350 °C, under atmospheric pressure). These results show that such molybdenum oxide is an attractive catalyst to selectively produce aromatics from oxygenated phenolic compounds. Unfortunately, a strong deactivation of Mo-based catalysts occurred during HDO reactions at atmospheric pressure [9,13–15]. For example, the conversion of *m*-cresol decreased about 25% in 7 h when reaction was performed at 350 °C under atmospheric pressure with unsupported MoO_x catalyst [13]. In the same way and under similar experimental conditions (320 °C, atmospheric pressure), supported MoO_x catalysts presented a significant deactivation (close to 50% after 14 h on stream when using $\text{MoO}_x/\text{TiO}_2$ catalyst) [14]. Such deactivation was attributed to coke deposition and/or over reduction of Mo leading to less or inactive Mo species. However, Prasomsri et al. [9] observed a significant enhancement in the stability of MoO_x -based catalysts during the HDO of 2-hexanone by increasing the partial pressure of H_2 , all experiments were carried out under atmospheric pressure. The beneficial effect of the increase of hydrogen partial pressure was attributed to both regeneration of oxygen vacancies, considered as active sites, and decrease in coke formation. From these results, performing HDO reactions under high hydrogen pressure can be an attractive approach to limit catalyst deactivation.

The present study concerns the evaluation of the deoxygenation catalytic properties (activity, selectivity and stability in reaction) of supported MoO_x catalysts under high pressure. The HDO of *m*-cresol used as a model oxygenated molecule was carried out at 340 °C under 4 MPa as total pressure over molybdenum oxides supported on different solids (commercial SiO_2 , synthetized SBA-15 and commercial $\gamma\text{-Al}_2\text{O}_3$). The impact of some characteristics of the support used on catalytic properties can then be considered.

2. Experimental

2.1. Catalyst preparation

Molybdenum oxide was obtained by incipient wetness impregnation (IWI), over both commercial supports (SiO_2 and $\gamma\text{-Al}_2\text{O}_3$) and ordered type silica (SBA-15). Active phase loading was fixed at 10 wt.% of Mo. SBA-15 was prepared under classical acidic conditions as initially proposed by Zhao et al. [18]. The detailed synthesis procedure can be found elsewhere [19]. For the IWI step, the calculated weight of the Mo precursor (ammonium molybdate tetrahydrate, $(\text{NH}_4)_6\text{Mo}_7\text{O}_{24}\cdot 4\text{H}_2\text{O}$, Sigma-Aldrich) was dissolved in known volumes, corresponding to measured water pore volume of the support. Thereafter, the prepared solution was added drop-wise to the corresponding support. After adding, the mixture was aged during 5 days at 25 °C. After drying, the samples were calcined at 400 °C (1.5 °C min^{−1}) for 5 h. Afterwards, the obtained catalysts were pelleted, crushed and sieved (250–315 µm).

2.2. Reaction setup

The hydrodeoxygenation of *m*-cresol was chosen to evaluate the influence of the support (nature and textural properties) on the catalytic properties of supported MoO_x catalyst. The catalytic test was performed in a down flow tubular inox fixed-bed reactor (length: 40 cm; inner diameter: 1.26 cm) operating at 4 MPa of total pressure. Prior to reaction, the catalysts (120 mg) were pretreated with pure H_2 (4.7 NL h^{−1}) at 340 °C for 30 min under 4 MPa as total pressure. The main purpose of this pre-treatment was to avoid the induction phase observed by Prasomsri et al. [13] during the HDO of *m*-cresol. The reaction was carried out at this temperature, in order to avoid an over-reduction of molybdenum species. The liquid feed, introduced in the reactor by using a HPLC Gilson pump, was composed by *m*-cresol as reactant (53 kPa), *n*-heptane as an internal standard (31 kPa) in dodecane. The $\text{H}_2/\text{m-cresol}$ ratio was set to 486 NL/L, the H_2 flow varied from 2.7 to 7.0 NL h^{−1} and the liquid feed flow from 5.55 to 14.40 mL h^{−1}. The H_2 partial pressure is equal to 3.2 MPa in reaction conditions. The line at the bottom of the reactor was maintained at 10 °C using a Minichiller-Huber condenser. Thus, liquid samples were collected every hour and analyzed using a Varian 430 chromatograph equipped with a DB1 capillary column (length: 30 m; inside diameter: 0.320 mm; film thickness: 5 µm) and a FID detector.

Conversion and selectivity were calculated by Eqs. (1) and (2) as follows:

$$X_{\text{CRE}} (\%) = \frac{C_{\text{CRE},0} - C_{\text{CRE}}}{C_{\text{CRE},0}} \cdot 100 \quad (1)$$

$$S_i (\text{mol}\%) = \frac{C_i}{C_{\text{CRE},0} - C_{\text{CRE}}} \cdot 100 \quad (2)$$

where $C_{\text{CRE},0}$ and C_{CRE} are the molar fractions of *m*-cresol in the feed and in the collected liquid sample; C_i is the molar fraction of a given i product.

Space times (τ in g hmol^{-1}) were calculated from the catalyst weights and the *m*-cresol flow as defined in Eq. (3):

$$\tau = \frac{w}{F_{\text{CRE}}} \quad (3)$$

with w as the weight of catalyst (120 mg), and F_{CRE} , the molar flow of *m*-cresol.

A first-order model was used to evaluate the rate constant of the transformation of *m*-cresol. Thus, the overall apparent rate constant (k_{HDO}) was calculated by Eq. (4):

$$k_{\text{HDO}} = \frac{1}{\tau} \ln(1 - X_{\text{CRE}}) \quad (4)$$

where k_{HDO} is the reaction rate constant ($\text{mmol g}^{-1} \text{h}^{-1}$).

2.3. Characterization of fresh and activated catalysts

The molybdenum loading in catalysts was determined by atomic absorption AA200 Perkin Elmer. The wavelength used was 313.26 nm. Before analysis, the catalysts were solubilized in an acidic aqueous solution containing both hydrochloric and nitric acids.

The textural properties (surface areas, pore volume and pore size) of the support and as-prepared catalysts were obtained by N_2 physisorption at −196 °C. Surface areas (using the B.E.T. method) and pore size (B.J.H. method) were issued from adsorption-desorption isotherms. Prior to the analysis, samples were outgassed at 200 °C overnight to remove any surface adsorbed residual moisture.

The XRD patterns of the bare supports and Mo supported catalysts were obtained on a PANalytical EMPYREAN powder

Table 1Chemical composition and textural properties of bare supports and impregnated MoO_x catalysts.

Solid	Mo ^a (wt.%)	S_{BET} ^b ($\text{m}^2 \text{g}^{-1}$)	Pore volume ^c ($\text{cm}^3 \text{g}^{-1}$)	Average pore diameter ^d (nm)
SiO_2	–	271	0.40	9
$\text{MoO}_x/\text{SiO}_2$	10.2	253 (299) ^e	0.62 (0.73) ^e	14
SBA-15	–	797	1.00	7
$\text{MoO}_x/\text{SBA-15}$	9.1	586 (678) ^e	0.72 (0.83) ^e	6
Al_2O_3	–	251	0.77	12
$\text{MoO}_x/\text{Al}_2\text{O}_3$	10.5	216 (256) ^e	0.62 (0.73) ^e	12

^a Deduced from atomic absorption.^b Specific surface area calculated by the BET method.^c Total pore volume determined at $P/P_0 = 0.98$.^d Calculated using the adsorption branch from the N_2 isotherm.^e In brackets are values determined after correction due to the contribution of the weight gain consecutive to the introduction of MoO_3 .

diffractometer in Bragg-Brentano ($\theta-\theta$) configuration with a copper tube powered at 45 kV and 40 mA ($\text{Cu K}\alpha 1 = 1.54060 \text{\AA}$ and $\text{Cu K}\alpha 2 = 1.54443 \text{\AA}$). A nickel filter was installed in the secondary optic in order to eliminate the $\text{K}\beta$ component. Analysis is performed for 2θ values from 20° to 80° , with steps of 0.1° and fixed acquisition time of 20 min per step. Low angles diffractions were also collected from 0.5° to 5° for SBA-15 and derived catalyst. Obtained diffractograms were analyzed with HighScore Plus software. Before analysis, a pretreatment was performed at 340°C (5°C min^{-1}) under 4 MPa of hydrogen for 30 min (flow of $\text{H}_2 = 4.7 \text{ NL h}^{-1}$).

The H_2 -TPR profiles of the Mo-based catalysts were collected on a Micromeritics AutoChem 2910 from 100°C to 1000°C using a ramp of 5°C min^{-1} , under 10 vol.% H_2 in Ar flow (total flow rate of 20 mL min^{-1}). Prior to the experiments, samples were pretreated with pure He (20 mL min^{-1}) at 200°C during 1 h. The hydrogen consumption was continuously monitored using TCD.

NH_3 -TPD was performed for each supported MoO_x . Experiments were performed on a Micromeritics AutoChem 2910 equipment. Prior to the experiments, samples were pretreated with pure He at 200°C for 1 h. After treatment, the temperature was lowered to 100°C and the sample was saturated with anhydrous NH_3 (10 vol.% in He) for 1 h. Subsequently, the samples were purged under He flow, and the temperature was raised to 600°C applying a temperature gradient rate of 5°C min^{-1} . The desorbed NH_3 was continuously monitored by TCD.

Raman spectra were recorded using HORIBA JOBIN YVON Labram HR800UV and an argon ion laser (Melles Griot) with an excitation wavelength of 514.5 nm. A laser power of 0.4 mW at the sample was applied.

The TEM studies were performed on a JEOL 2100 UHR 200 kV microscope equipped with a Gatan Ultra scan camera. Samples were dispersed ultrasonically in ethanol and deposited on a copper grid supporting a perforated carbon film.

Oxygen chemisorption was performed for each solid. Before analysis, the materials were activated using the following standard procedure: 340°C under 4 MPa of hydrogen during 30 min. The solid was inserted in a quartz U-shaped tube reactor. Successive pulses of pure O_2 at 340°C were then injected until saturation of the sample. The O_2 uptake (oxygen adsorbed) was used to calculate the number of redox active Mo species (Eq. (5)) and the TOF (Turn over Frequency, in h^{-1} – Eq. (6)), as proposed by Shetty and co-workers [14].

$$\% \text{ Redox Mo} = \frac{2. \text{ Oxygen uptake}}{\text{Mo loading}} \cdot 100 \quad (5)$$

$$\text{TOF} = \frac{k_{\text{HDO}}}{2. \text{ Oxygen uptake}} \cdot 100 \quad (6)$$

2.4. Characterization of spent catalysts

Chemical analysis of carbon and hydrogen were carried out after reaction test by using an elemental analyzer (NA2100 ana-

lyzer, CE instruments). XRD analysis were also performed over all spent catalysts. These catalysts were characterized without chemical treatment.

3. Results and discussion

3.1. Catalyst characterization

As indicated in Table 1, the experimental molybdenum loadings, determined by atomic absorption, were close to the set value of the preparation, i.e. 10 wt.%. Fig. S1 in the Supplementary Information shows the N_2 adsorption-desorption isotherms for the bare supports and MoO_x derived catalysts. Both $\text{MoO}_x/\text{SBA-15}$ and $\text{MoO}_x/\text{Al}_2\text{O}_3$ catalysts presented similar profiles (type IV isotherms) compared to their respective supports, indicating porosity developed in the domains of the mesopores. In addition, the hysteresis shapes did not evolve after the impregnation-activation step. This result indicates that the pore characteristics remains unchanged for the supported molybdenum materials. However, the N_2 physisorption isotherms obtained for bare SiO_2 and $\text{MoO}_x/\text{SiO}_2$ were quite different, evolving from type II to type IV. In addition, the hysteresis is also evolving due to a modification of pore shape from aggregate-type porosity to ink-bottle shaped porosity. Such important modification of the pore characteristics, upon aqueous impregnation, was already reported by Sydorchuk et al. [20] over commercial silica.

Calculated values of specific surface area, pore volume, and pore diameter issued from physisorption isotherms, are gathered in Table 1. As expected, the surface specific area of $\text{MoO}_x/\text{SBA-15}$ was the highest (equal to $586 \text{ m}^2 \text{ g}^{-1}$). For supported molybdenum materials, raw values were recalculated to remove the contribution of MoO_3 weight on textural properties (values in parenthesis in Table 1) and to access information on the stability of the support during impregnation-calcination steps [21]. The corrected surface areas obtained for $\text{MoO}_x/\text{SiO}_2$ and $\text{MoO}_x/\text{Al}_2\text{O}_3$ were close to those displayed by the parent support, and range around 250 – $300 \text{ m}^2 \text{ g}^{-1}$. No notable modification of the surface area between the support and the catalyst indicates, for these two materials, a satisfying stability of the support was observed, even for the silica derived catalyst for which important modification of the isotherm shape. On the contrary, the corrected surface area of $\text{MoO}_x/\text{SBA-15}$ was lower than the surface area of SBA-15 (decreased by 15%). The decrease can originate from possible pore plugging occurring when confined particles forms during the calcination steps [22,23]. Considering the pore volume values, the corrected value of $\text{MoO}_x/\text{Al}_2\text{O}_3$ was close to the one measured on the parent support (around $0.7 \text{ cm}^3 \text{ g}^{-1}$), whereas the corrected value of $\text{MoO}_x/\text{SBA-15}$ was lower compared to its bare support (decreased by 15%). This result is always in favor of the formation of mesopore confined particles in the SBA-15 channel type porosity. On the contrary, the presence of MoO_x phase allowed to increase the pore volume (by about 80%) of SiO_2 .

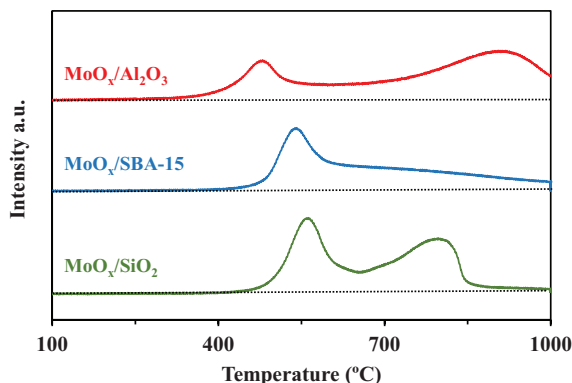


Fig. 1. $\text{H}_2\text{-TPR}$ profiles of supported MoO_x catalysts.

Finally, the catalysts pore size average is only slightly modified by the impregnation-activation process except for the SiO_2 materials for which significant modification of the isotherm shape was observed.

XRD patterns of calcined supports and catalysts activated at 340°C under 4 MPa of H_2 , are presented in Fig. S2 (Supplementary Information). Over silica-based catalysts, only a broad reflection was observed, at $20 \sim 22^\circ$, characteristic of amorphous silica. For alumina based support, only reflections ascribed to $\gamma\text{-Al}_2\text{O}_3$ were detected [24]. Regardless of the support used, reflections attributed to MoO_x phase were never observed, which suggests that molybdenum oxide forms small particles ($<3\text{-}4 \text{ nm}$, detection limit of the X-ray diffraction), and/or remains in an amorphous state. For SBA-15 loaded molybdenum oxide, low angle XRD was performed (Fig. S3, Supplementary Information). The presence of three reflections at $20 > 2^\circ$ is a clear indication of the maintaining of the hexagonal pore structure in the catalyst, as awaited from N_2 physisorption result interpretation (Fig. S1). Decrease in intensity and small variation in peak position, over the $\text{MoO}_x/\text{SBA-15}$, is originated from reduction of contrast and strong X-ray absorption from heavier molybdenum atoms [25].

In order to obtain Supplementary information concerning the size of molybdenum oxide particles, representative images obtained for the three Mo-containing catalysts are presented in the Supplementary Information file (Figs. S4–S6). On SiO_2 , molybdenum oxide particles were observed as both microparticles (diameter close to $1 \mu\text{m}$) and nanoparticles ($1\text{-}2 \text{ nm}$) as shown in Fig. S4. On SBA-15 (Fig. S5) and Al_2O_3 (Fig. S6), only pseudo-spherical MoO_x particles of very small sizes ($1\text{-}2 \text{ nm}$ for $\text{MoO}_x/\text{SBA-15}$ and lower than 1 nm for $\text{MoO}_x/\text{Al}_2\text{O}_3$) located on the support surfaces were observed. Thus, the use of either an ordered silica (SBA-15), or an acidic support (alumina) instead of SiO_2 favored the dispersion of molybdenum oxide species, preventing the formation of very large particles of MoO_x . In addition, EDX analysis confirms a molybdenum loading on local analysis zone comparable to this awaited from chemical analysis.

TPR profiles of MoO_x based catalysts are presented in Fig. 1. Reducibility of molybdenum was strongly dependent on the support nature and morphology. First, over silica and alumina, Mo(VI) can be present in both octahedral (Mo_0) and tetrahedral (Mo_T) forms [26]. Reduction of MoO_3 phase proceeds in two steps, with a first reduction of MoO_3 into MoO_2 (in the range of $450\text{-}650^\circ\text{C}$) followed by the reduction of MoO_2 into molybdenum metal (up to 700°C) [27]. For the three samples, the observed low temperature (LT) reduction is assigned to the partial reduction of octahedrally coordinated Mo(VI) into Mo(IV) [28]. The temperature of the LT reduction of supported molybdenum oxides followed: $\text{MoO}_x/\text{Al}_2\text{O}_3$ ($\sim 475^\circ\text{C}$) $<$ $\text{MoO}_x/\text{SBA-15}$ ($\sim 540^\circ\text{C}$) $<$ $\text{MoO}_x/\text{SiO}_2$ ($\sim 560^\circ\text{C}$). This indicates that Mo(VI) species are more easily reducible on Al_2O_3 .

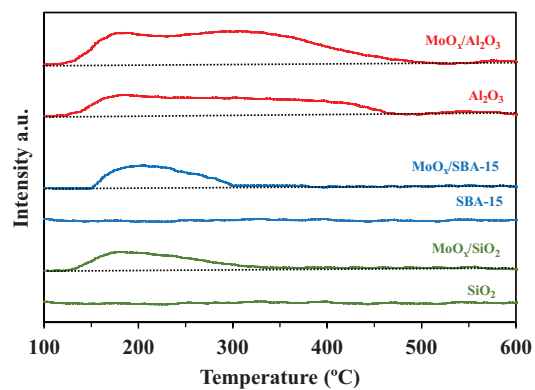


Fig. 2. $\text{NH}_3\text{-TPD}$ profiles of bare supports and supported MoO_x catalysts.

than on silica based supports, probably due to the smaller oxide particles as observed by TEM (Figs. S4–S6). A second reduction peak was also observed at higher temperatures, particularly for molybdenum oxides supported on Al_2O_3 and SiO_2 . These peaks can be ascribed to a deep reduction of residual Mo(VI) and Mo(IV) into Mo^0 , including highly dispersed Mo_T from MoO_3 phase [28]. Table 2 shows the values hydrogen consumed obtained by $\text{H}_2\text{-TPR}$ experiments, and theoretical hydrogen consumption to reduce all Mo(VI) to metal. Over silica, a reduction degree of about 80% was calculated, showing an incomplete reduction of molybdenum cation, even at 1000°C , which could be related to the presence of oxide microparticles (Fig. S4). Higher molybdenum reduction degree (higher than 90%) was determined when molybdenum oxides were supported over alumina. In addition, the molybdenum oxide species were less reducible to metallic Mo on alumina, since TPR experiments showed that the complete reduction occurred at the higher temperature (above 1000°C). This phenomena can be explained by smaller oxide particles on this support, as observed by TEM.

The acid properties of the MoO_x -based catalysts were probed using NH_3 thermodesorption experiments ($\text{NH}_3\text{-TPD}$). Although ammonia thermodesorption does not allow to discriminate Brønsted and Lewis acid sites, the amount of NH_3 desorbed is an indirect measure of the material global acidity. Acidity of the molybdenum oxide phase was issued from the difference in global acidity between catalyst and support. Profiles for bare and impregnated supports are presented in Fig. 2. As expected, both SiO_2 and SBA-15 did not present any significant NH_3 desorption. Al_2O_3 support exhibited both weak ($<300^\circ\text{C}$) and intermediate/strong ($>300^\circ\text{C}$) acidity. $\text{NH}_3\text{-TPD}$ experiments performed over Mo-containing catalysts display an increase of the acidity for all solids, which can be attributed to the presence of the molybdenum oxide phase. Over these materials, the amount of ammonia desorbed ranges between $658 \mu\text{mol g}^{-1}$ and $860 \mu\text{mol g}^{-1}$ (Table 2). As proposed by several authors [29,30], the MoO_x phase exhibits mainly Brønsted acid sites caused by the formation of hydroxyl groups on the molybdenum oxide layers.

Oxygen uptake measurement was used to determine the number of active Mo species. As described by Shetty et al. [14] molybdenum is expected to be present at the +VI oxidation number when supported over silica and alumina supports. These authors demonstrated that the oxygen chemisorption experiments was an efficient technique to evaluate the number of oxygen vacancies, coordinately unsaturated sites (CUS) involved in HDO. Active site number thereafter allows to calculate TOF values of different MoO_x -based catalysts. Oxygen uptake values, issued from oxygen chemisorption experiments are gathered in Table 2, and the following order of uptake is obtained: $\text{MoO}_x/\text{Al}_2\text{O}_3 > \text{MoO}_x/\text{SBA-15} > \text{MoO}_x/\text{SiO}_2$. This order is identical to the order of Mo(IV) reducibility, as observed from TPR experiments

Table 2

Physico-chemical characterizations of bare supports and impregnated MoO_x catalysts.

Solid	H_2 uptake (mmol g^{-1})		MoO_x Reducibility (%)	Total acidity ^c ($\mu\text{mol g}^{-1}$)	O_2 uptake ^d ($\mu\text{mol g}^{-1}$)	Redox Mo ^e (%)
	Exp. ^a	Cal. ^b				
SiO_2	n.d.	n.d.		0	0	n.d.
$\text{MoO}_x/\text{SiO}_2$	2.7	3.2	84	860	115	22.1
SBA-15	n.d.	n.d.		0	0	n.d.
$\text{MoO}_x/\text{SBA-15}$	2.3	2.9	79	708	163	31.3
Al_2O_3	n.d.	n.d.		1044	0	n.d.
$\text{MoO}_x/\text{Al}_2\text{O}_3$	3.1	3.3	94	1702	181	34.7

^a Quantity of H_2 determined from TPR experiments.

^b Quantity of H_2 calculated according the nominal composition according the following reaction: $\text{MoO}_3 + 3\text{H}_2 \rightarrow \text{Mo} + 3\text{H}_2\text{O}$.

^c Deduced from NH_3 -TPD.

^d Deduced from chemisorption of O_2 .

^e Calculated using Eq. (5).

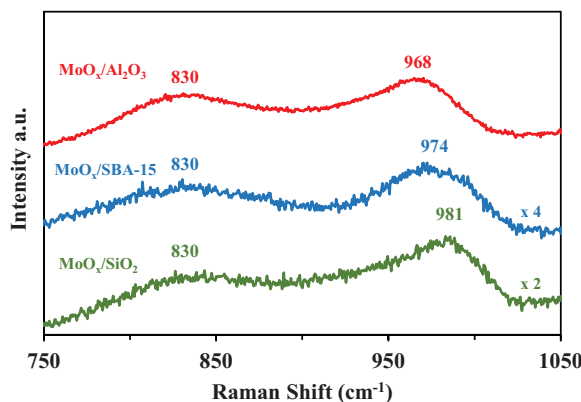


Fig. 3. Raman spectra of supported MoO_x catalysts in the Raman shift ranges of 750–1050 cm^{-1} .

(Fig. 1), and seems to be related to the difference in molybdenum oxide particle size on the three catalysts. No oxygen uptake was observed over bare supports.

Raman spectra of the catalysts, recorded in the 750–1050 cm^{-1} domain, are presented in Fig. 3. Two main signals were observed: (1) at 968–981 cm^{-1} , characterizing $\text{Mo}=\text{O}$ terminal stretching vibration, and (2) a broad band at $\sim 830 \text{ cm}^{-1}$ located in the region to $\text{Mo}-\text{O}-\text{Mo}$ functionalities [31–35]. A variation of the band position ascribed to the $\text{Mo}=\text{O}$ stretching vibration is observed depending on the support. For $\text{MoO}_x/\text{Al}_2\text{O}_3$, the band was positioned at 968 cm^{-1} . For $\text{MoO}_x/\text{SiO}_2$, its position was at 981 cm^{-1} , while an intermediate value was obtained for $\text{MoO}_x/\text{SBA-15}$ (974 cm^{-1}). The shift could be linked to the differences in vacancy densities in the MoO_x clusters. Regarding the results of H_2 -TPR and oxygen chemisorption measurements, it seems that when Raman signal of $\text{Mo}=\text{O}$ terminal stretching vibration appears at lower position, the vacancy densities increases and a higher Mo(VI) reducibility can be expected.

3.2. Catalytic properties of MoO_x -based catalysts on the hydrodeoxygenation of m-cresol

The hydrodeoxygenation of m-cresol was studied at 340 °C under 4 MPa as total pressure over the three MoO_x supported catalysts. A blank test was performed showing that m-cresol was unreactive in absence of catalyst. Similarly, the bare supports appeared to be inactive even at high τ values, with no measurable conversion of m-cresol. All experiments were carried out during 20 h on stream and τ (space time, as defined in Eq. (3)) was changed every 5 h to obtain different levels of conversion (Fig. 4). For all catalysts, it can be observed that the conversions obtained in the first 5 h were very close to those measured during the last 5 h on

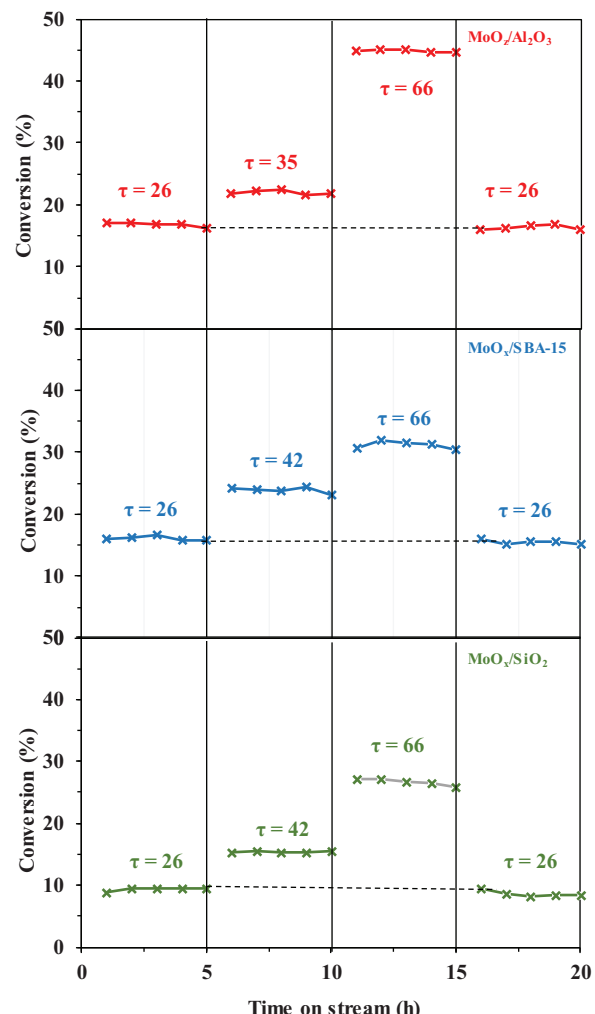


Fig. 4. Conversion as function of time on stream for the HDO of m-cresol at 4 MPa and 340 °C. $\text{MoO}_x/\text{SiO}_2$ (green); $\text{MoO}_x/\text{SBA-15}$ (blue); $\text{MoO}_x/\text{Al}_2\text{O}_3$ (red); τ in $\text{mol g}^{-1}\text{h}^{-1}$.

stream when τ remains constant (equal to 26 g h mol^{-1}), experiments being carried out under high pressure, i.e. 3.2 MPa of H_2 . This indicates an absence of catalyst deactivation/poisoning during reaction for at least 20 h, which reflects a satisfying stability for the molybdenum active sites. The amounts of carbon contained in the used catalysts was relatively high (between 4.7 and 6.9 wt%, as indicated in Table 3). Carbon can be related to adsorbed molecules on the catalyst surface. The nature of organic molecules can be identified, based on the measured C/H ratio in weight basis [36]. For all catalysts, these values were close to 10.5, which is the C/H ratio of

Table 3

Chemical composition in carbon and hydrogen of spent catalysts.

Catalyst	C (wt.%)	H (wt.%)	C/H
MoO _x /SiO ₂	6.6	0.7	10
MoO _x /SBA-15	6.9	0.8	9
MoO _x /Al ₂ O ₃	4.7	0.4	12

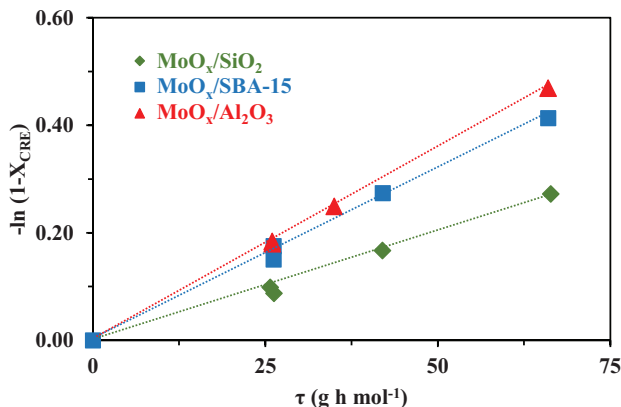


Fig. 5. Plots of $-\ln(1-X_{CRE})$ as function of τ obtained from the HDO of *m*-cresol at 4 MPa and 340 °C. MoO_x/SiO₂ (◆); MoO_x/SBA-15 (●); MoO_x/Al₂O₃ (▲).

m-cresol. Consequently, carbon in the spent catalysts is preferably attributed to the presence of adsorbed phenolic reactant on the catalyst surface. The presence of coke formed during reaction cannot however be completely excluded. However, if carbon massively formed during reaction, the C/H experimental ratio should have been significantly higher than 10. Such stability was clearly not the case when HDO reactions using molybdenum oxide was performed under atmospheric pressure, where MoO_x based catalysts exhibited poor stability [14]. Such beneficial effect of H₂ pressure on the catalyst stability was recently highlighted over a phosphide catalyst (Ni₂P) for HDO reaction [36]. The observed deactivation of MoO_x based catalysts was attributed both to the over reduction of Mo(VI) into less active species and to coke deposition on catalyst surface [9,14]. In our case, it seems that the use of high pressure results in several beneficial effects: (i) there is no induction period for reaction, as observed by Prasomsri et al. [13], and (ii) the stability of catalysts is improved.

Fig. 5 shows a linear relationship between $\ln(1-X_{CRE})$ and τ , which indicates a first order reaction for HDO of *m*-cresol over supported molybdenum oxides. The k_{HDO} values obtained using Eq. (9) showed the following order of activity for materials: MoO_x/Al₂O₃ > MoO_x/SBA-15 > MoO_x/SiO₂ (Table 4). The nature of the support for MoO_x acted positively on the active sites numbers, which are proposed to be coordinatively unsaturated sites (CUS) [9,14]. Such increase in CUS density in material was demonstrated by O₂ chemisorption. The O₂ uptake (Table 2) followed the same order as the deoxygenation activity. In addition, the fact that MoO_x/SiO₂ was less active than MoO_x/SBA-15 can be explained by the presence of large microparticles of MoO_x over the former which were probably less active than MoO_x nanoparticles for the HDO reaction.

It is noteworthy that molybdenum in sulfide phase was about 1.6 times more active than in oxide phase [37], demonstrating a higher activity of MoS₂ compared to the MoO_x. This fact may be explained by either an easier formation of a sulfur vacancy than an oxygen vacancy on molybdenum or differences in strength between these two CUS. Nevertheless, it must be emphasized that a sulfur source (dimethyldisulfide) was added in the model feed to maintain the catalytic activity of MoS₂/Al₂O₃ stable, preventing the oxidation of the sulfide phase [38]. Since sulfur is present at very low contents

in biomass feedstocks [39], sulfide catalysts are likely to deactivate during HDO. Moreover, the strategy of adding sulfur to a biomass feedstock would lead to the eventual contamination of the products [11,12], which is indeed not desired.

Table 5 shows the distribution of products obtained from *m*-cresol HDO over the three MoO_x based catalysts at comparable levels of conversion (about 20%). Interestingly, all detected products were deoxygenated, which point out that MoO_x based catalysts are efficient catalysts for deoxygenation reactions. It was reported that alcohols and ketones, as oxygenated intermediates from *m*-cresol HDO, were observed over Ni₂P/SiO₂ catalysts under comparable experimental conditions [36]. In addition, these intermediates were usually observed when noble (i.e. Pd, Pt) or non-noble catalysts (i.e. Ni, Co) were used for the HDO of phenolic molecules [40,41]. Regardless of the support nature, toluene was the main deoxygenated product, accounting for more than 80 mol% of all deoxygenated products. Similarly, Shetty et al. [14] previously reported that the use of MoO_x based catalysts led only to aromatics production during the HDO of *m*-cresol under atmospheric pressure. It is noteworthy to mention that the relative high pressure of H₂ used in our work allowed to maintain high selectivity into aromatics, while methylcyclohexenes were also observed at low selectivity and methylcyclohexane appeared as trace. Indeed, methylcyclohexenes selectivity ranged between 11 and 15 mol% and methylcyclohexane was clearly the minor product, its selectivity being always below 5 mol%. As presented in Table 4, the 1-MCH_e/MCH_{es} ratio ranged between 60 and 65 mol%, showing that 1-methylcyclohexene was always the main alkene isomer observed from *m*-cresol HDO, in accordance with results reported over sulfide [37] and phosphide [36] catalysts. From a thermodynamic point of view, at 340 °C, the ratio of 1-methylcyclohexene/methylcyclohexenes, is expected to be equal to 65 mol% [42]. It is noteworthy to mention that 1-methylcyclohexene is not directly expected from *m*-cresol. Indeed, it can be assumed that the total hydrogenation of the aromatic ring of *m*-cresol leads only to 3-methylcyclohexanol. This alcohol was never detected during reaction. TPD-NH₃ experiments (Fig. 2) highlighted the formation of acid sites attributed to the molybdenum oxide species, which can dehydrate this alcohol into either 3- or 4-methylcyclohexenes. The fact that 1-methylcyclohexene appeared as the main alkene isomer, implies that an isomerization step occurred, involving the acid properties of the MoO_x phase. In the case of MoO_x/Al₂O₃, isomerization might also occur on alumina acid sites.

Table 5 also presents the product distribution determined over MoS₂/Al₂O₃ [37]. Over such phase, the deoxygenation of *m*-cresol mainly led to hydrogenated products, methylcyclohexenes being the main products. This indicates a completely different behavior between molybdenum oxide and sulfide phases, the former being very selective to aromatic whereas the latter was selective into cycloalkenes and cycloalkanes. Consequently the nature of a sulfur vacancy and an oxygen vacancy could be different in nature, the former favoring the hydrogenation of aromatic ring whereas the latter favoring the direct C–O bond scission.

Based on the distribution of the products, a reaction scheme for the HDO of *m*-cresol over molybdenum oxides supported catalysts, under high H₂ pressure, is depicted in Scheme 1. The same reaction scheme was also proposed to explain the formation of deoxygenated products over sulfide phases [37]. Thus, two reaction routes were proposed: Direct DeOxygenation (DDO route) and ring HYDrogenation (HYD route). The main pathway involves the direct cleavage of the C–O bond of *m*-cresol leading to toluene production. The HYD route is responsible for the formation of methylcyclohexenes and methylcyclohexane. This latter and minor pathway was never previously observed over such MoO_x catalysts [9,13,14],

Table 4

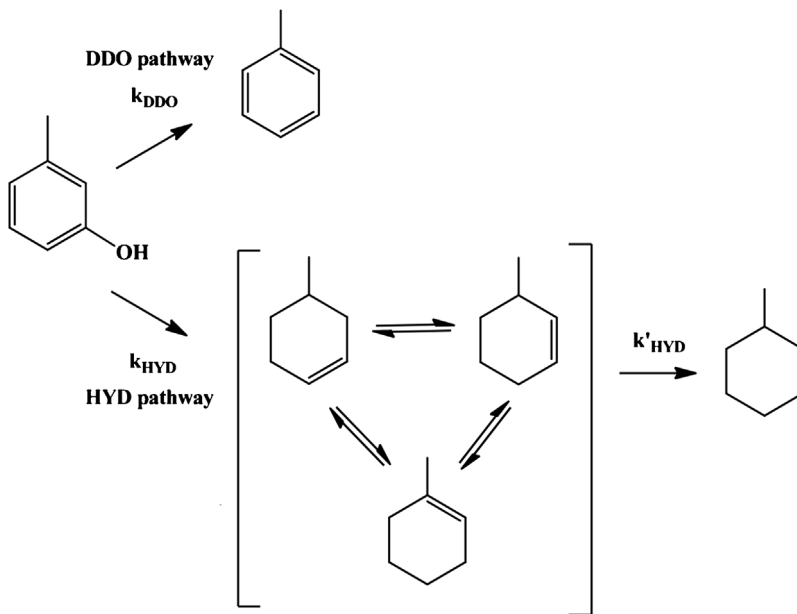
Individual apparent rate constants and TOF values (standard deviation of values close to 5%) determined during the transformation of *m*-cresol over molybdenum oxides based catalysts at 340 °C under 4 MPa of total pressure.

	Rate constants (in mmol g ⁻¹ h ⁻¹)				TOF (h ⁻¹)
	k _{HDO}	k _{DDO}	k _{HYD}	k' _{HYD}	
MoO _x /SiO ₂	4.1 ± 0.2	3.4 ± 0.2	0.70 ± 0.03	12.3 ± 0.6	19 ± 1
MoO _x /SBA-15	6.5 ± 0.3	5.4 ± 0.3	0.90 ± 0.04	8.6 ± 0.4	20 ± 1
MoO _x /Al ₂ O ₃	7.1 ± 0.3	6.1 ± 0.3	1.00 ± 0.05	6.9 ± 0.3	20 ± 1
MoS ₂ /Al ₂ O ₃ [37]	11.6 ± 0.6	3.2 ± 0.2	8.4 ± 0.4	37.1 ± 1.8	n.d.

Table 5

Product distribution from the HDO of *m*-cresol at 340 °C under 4 MPa of total pressure over supported molybdenum oxides and sulfide catalysts.

Catalyst	τ (g h mol ⁻¹)	Conversion (%)	Selectivity (mol%)			1-MCHe/ MCHeS
			Tol	MCHeS	MCH	
MoO _x /SiO ₂	66.0	23.8	81.9	14.9	3.2	60
MoO _x /SBA-15	42.0	23.9	82.8	14.3	2.9	60
MoO _x /Al ₂ O ₃	35.0	22.1	85.5	12.8	1.7	65
MoS ₂ /Al ₂ O ₃ [37]	15.8	16.9	27.8	53.6	18.6	65

**Scheme 1.** Reaction network of *m*-cresol transformation at 340 °C and 4 MPa over supported MoO_x.

probably because these studies were carried out under atmospheric pressure.

In turn, a kinetic modeling was performed in order to better evaluate the effect of supporting molybdenum on different solids. Such model was already used to determine the kinetic values involved in the HDO of cresol isomers over sulfide catalysts [37]. The kinetic values determined (k_{DDO} , k_{HYD} and k'^{HYD}) are given in Table 4. For catalysts studied, k_{DDO} values (ranged from 3.4 to 6.1 mmol h⁻¹ g⁻¹) were higher than k_{HYD} values (between 0.7 and 1.0 mmol h⁻¹ g⁻¹), which is in accordance with the high selectivity to aromatics measured. In the model used, the hydrogenation of toluene into methylcyclohexane was not considered since the selectivity into toluene was independent of the conversion of *m*-cresol, irrespective to the catalyst as shown in Fig. 6. This assumption was confirmed with an additional experiment using toluene as reactant which showed that this aromatic was unreactive under our experimental conditions over MoO_x catalysts.

The product distribution obtained experimentally from the HDO of *m*-cresol over supported molybdenum oxides as well as the cal-

culated data are presented in Fig. 6, which displays a good data fitting for all catalysts. Regardless of the catalyst used, toluene and methylcyclohexenes were found as primary products, whereas methylcyclohexane appeared as a secondary product, accordingly the reaction scheme proposed (Scheme 1). According to values reported in Table 4, k_{HDO} , k_{DDO} and k_{HYD} followed the same order: MoO_x/Al₂O₃ > MoO_x/SBA-15 > MoO_x/SiO₂. This might suggest that active sites in both deoxygenation routes could be similar in nature. However, the order of k'^{HYD} values, which measure the hydrogenation capability of alkenes, followed the inverse order: MoO_x/SiO₂ > MoO_x/SBA-15 > MoO_x/Al₂O₃. This fact seems to indicate that active sites responsible for the hydrogenation of aromatic ring could be different in nature than those involved for the hydrogenation of alkenes.

An interesting difference in behavior between oxide and sulfide molybdenum phase is highlighted by the comparison between the rate constant values reported in Table 4. Indeed, the MoS₂ phase favors hydrogenation reactions in a large extend (compare k_{HYD} and k'^{HYD} values for both catalysts supported on alumina), whereas the

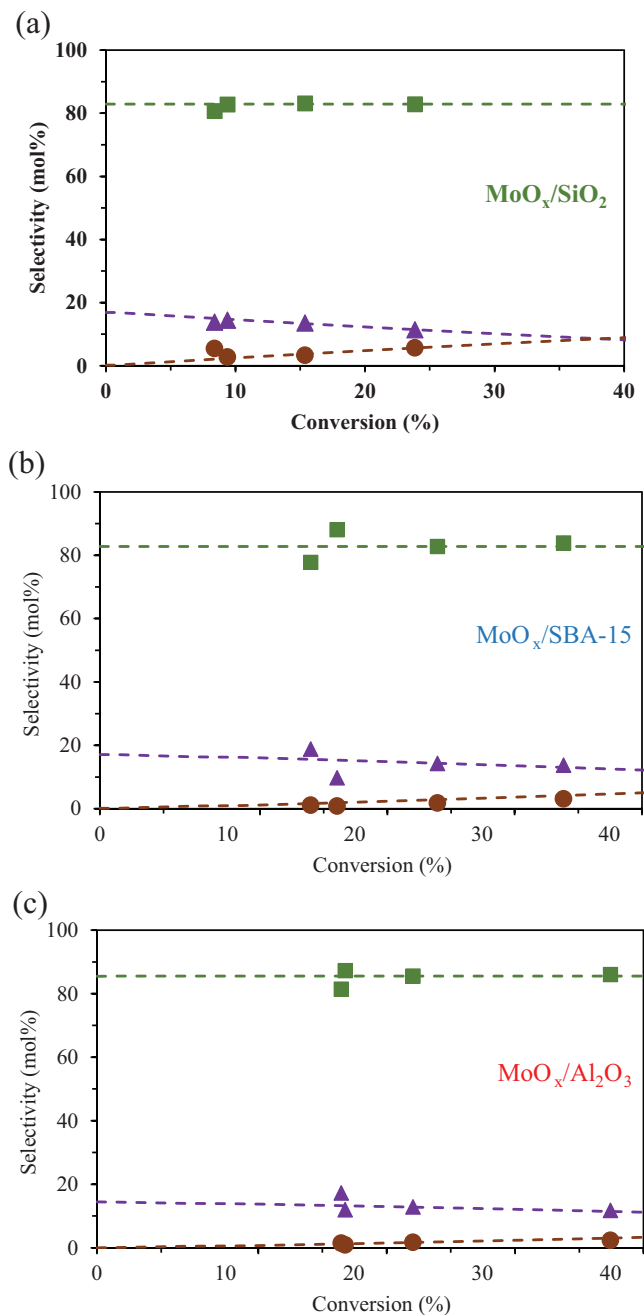


Fig. 6. Selectivity as function of *m*-cresol conversion. Experimental data obtained at 4 MPa and 340 °C using $\text{MoO}_x/\text{SiO}_2$ (a); $\text{MoO}_x/\text{SBA-15}$ (b); $\text{MoO}_x/\text{Al}_2\text{O}_3$ (c). Toluene (■); methylcyclohexenes (▲); methylcyclohexane (●). Calculated data (—).

rate of the C–O bond scission (k_{DDO}) determined on $\text{MoO}_x/\text{Al}_2\text{O}_3$ was about twice higher than the one measured over $\text{MoS}_2/\text{Al}_2\text{O}_3$. Such different results obtained over molybdenum sulfide catalysts compared to oxide shows an opposite trend which is in accordance to lower selectivity in aromatics measured over $\text{MoS}_2/\text{Al}_2\text{O}_3$. Moreover, these results are in line with the assumption that the active sites on both phases may be different.

3.3. Proposals on the nature of active sites and on the reaction mechanism

Although the specific nature of the HDO active sites present in molybdenum oxide phase needs further clarification, it can be proposed that oxygen vacancies involving reduced Mo species (Mo^{5+}

and Mo^{4+}) have a main role in deoxygenation reactions [9,13,14]. It was recently proposed that oxycarbide phase ($\text{MoO}_x\text{C}_y\text{H}_z$) could also participate as active site in HDO [13,14]. In our case, such species were only detected over the $\text{MoO}_x/\text{SiO}_2$ spent catalyst (Fig. S7, Supplementary Information). As this catalyst exhibited the lowest activity, the involvement of such species as HDO active sites remains uncertain.

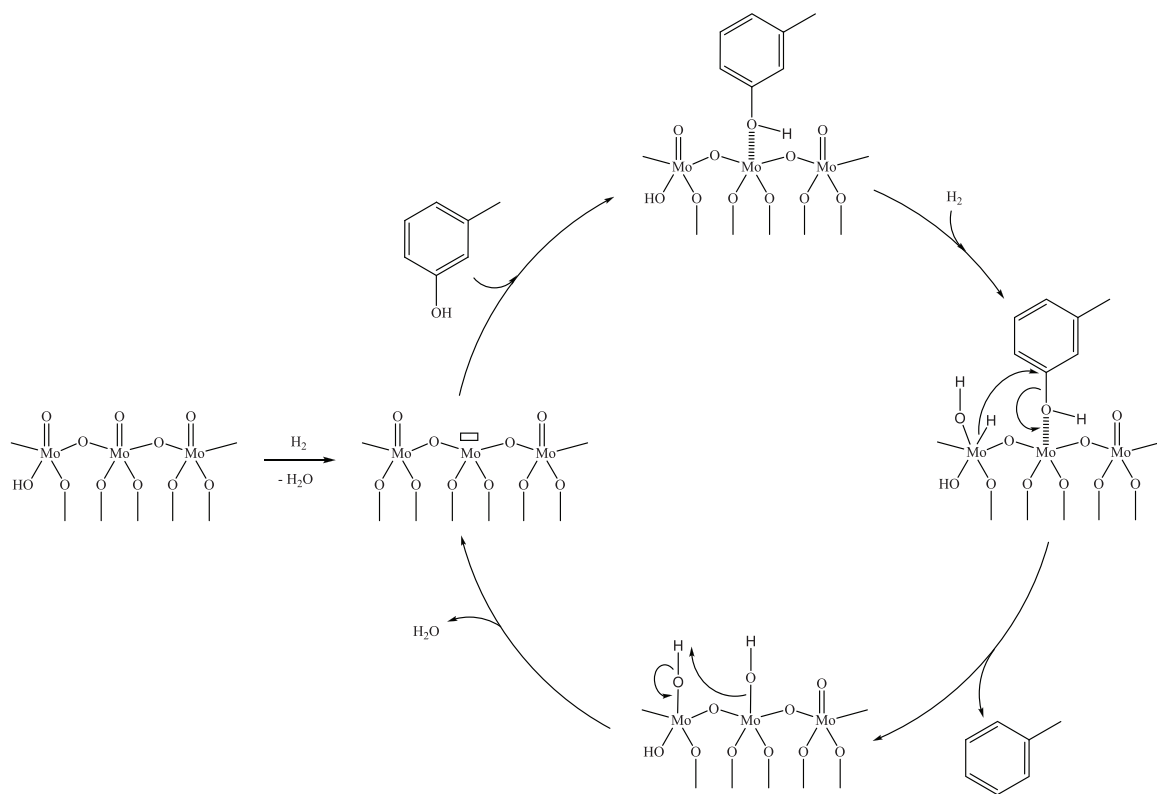
The formation of oxygen vacancy was estimated by DFT method using a Mo_3O_9 cluster model of the MoO_3 surface [9,43]. For example, it was proposed that the first step to create such vacancy is the adsorption of H_2 , followed by a proton transfer and finally the release of water, the overall process being endothermic (about 90 kJ mol⁻¹) [9]. The beneficial role of H_2 was confirmed experimentally for HDO of 2-hexanone over MoO_3 . Indeed, an increase of the partial pressure of H_2 resulted in better activity and stability of the catalyst, demonstrating that H_2 atmosphere allow to favor the creation of oxygen vacancies. According to the proposal of vacancies being the HDO active sites, it is hence necessary to remove an atom oxygen bonded to molybdenum. Therefore, it is expected that an easier reduction of Mo species provides a more available number of active sites due to an easier O-removal from the surface. From H_2 -TPR and chemisorption experiments (Fig. 1 and Table 2), it seems that the formation of such sites on molybdenum oxides is the most favored when Al_2O_3 is used as support and less favored when SiO_2 is the support. These proposals are in line with the experimental order of activity determined for the HDO of *m*-cresol: $\text{MoO}_x/\text{Al}_2\text{O}_3 > \text{MoO}_x/\text{SBA-15} > \text{MoO}_x/\text{SiO}_2$ (Fig. 5). Nevertheless, the turnover frequency values (TOF; Eq. (6)) of all catalysts were close to 20 h⁻¹ (Table 3), which indicates that all catalysts displayed similar intrinsic activities per site and hence suggests that the active sites involved in HDO of phenolic compounds are very similar in nature irrespective to the support used.

In addition, the fact that $\text{MoO}_x/\text{SBA-15}$ was more active than $\text{MoO}_x/\text{SiO}_2$ could be attributed to a better dispersion of molybdenum oxides on SBA-15 than on SiO_2 , as observed in TEM images (Fig. 3), and supported by the highest O_2 uptake determined for $\text{MoO}_x/\text{SBA-15}$ compared to $\text{MoO}_x/\text{SiO}_2$ (Table 2). These differences between both catalysts could be related to their textural properties, including a specific surface area about twice higher for $\text{MoO}_x/\text{SBA-15}$ compared to $\text{MoO}_x/\text{SiO}_2$ (Table 1).

Scheme 2 presents a mechanism proposal concerning the formation of toluene (DDO product) from *m*-cresol, which is the main product obtained over molybdenum oxides catalysts (Table 2). Irrespective to the support, molybdenum species can be present as a sub-monolayer forming polymolybdate phase including Mo^{6+} , as proposed by several authors [14,35,44]. These species can react with H_2 which leads to the creation of MoO_x species (Mo(IV) in Scheme 2) releasing H_2O [9,14]. The oxygenated reactant could be adsorbed through its oxygen atom on the oxygen vacancy to favor the cleavage of the C–O bond. The next step is the activation of H_2 , which could occur by heterolytic dissociation. The addition of a hydride species on the carbon bearing the OH group could lead to the C–O bond scission and hence the formation of toluene. The vacancy is afterwards recovered by release of water.

The formation of HYD products (methylcyclohexenes and methylcyclohexane) firstly requires the total hydrogenation of the aromatic ring, probably involving a flat adsorption of *m*-cresol through its aromatic ring. In this case, the involvement of at least two neighboring vacancies could be proposed as active site. Such site seems unlikely over molybdenum oxides phase explaining the low quantity of HYD products compared to the DDO product, irrespective to the catalyst.

The HYD products being the main observed products on the sulfide phase might be explained by an easier creation of multiple sulfur vacancies compared to the creation of oxygen vacancies on



Scheme 2. Mechanism of the direct deoxygenation (DDO) route of *m*-cresol on a schematic molybdenum oxide site species.

molybdenum, leading to higher activity in hydrogenation. Nevertheless, compared to a sulfur vacancy, an oxygen vacancy could lead to a stronger molybdenum site for the DDO route, acting as Lewis acid site, favoring the C–O bond scission, which explains the high selectivity to aromatic of the molybdenum oxide phase compared to the sulfide phase.

4. Conclusion

The present study showed that supported molybdenum oxides are promising HDO catalysts to produce selectively aromatics from phenolic compounds, with a high degree of deoxygenation. Regardless of the catalyst used, the selectivity into toluene from *m*-cresol was always higher than 80 mol%.

An influence of the nature of support was highlighted: the order of HDO activity being $MoO_x/Al_2O_3 > MoO_x/SBA-15 > MoO_x/SiO_2$. The effect of the support could be attributed to the difference in the reducibility of Mo(IV) species observed by H_2 -TPR. Compared to a commercial silica, the reducibility of molybdenum oxides was improved either by the use of an acidic support (Al_2O_3), or by the use of a mesoporous nanoparticles support (SBA-15). These differences in behavior were related to the particle size of molybdenum oxide, being smaller and more reducible on alumina. Consequently, the number of active sites present on the oxide phase, measured by O_2 chemisorption, was a function of the support used: it was the highest on MoO_x/Al_2O_3 and the lowest on MoO_x/SiO_2 . In addition, it can be assumed that in the case of existence of active sites affected by the support (i.e. monomeric site), these are probably exhibiting a weak activity with no significant contribution to the global activity as demonstrated by the constant TOF values obtained whatever the support.

It can be assumed that the nature of active sites was not affected by the support, the TOF values being independent on the type of catalyst. In addition, as all catalysts exhibited a remarkable stability

under the experimental conditions used, the use of a high pressure of hydrogen (3.2 MPa) allowed to preserve these active sites.

Based on results presented in this study, in order to improve activity, further evolution of the catalyst consists in the control of the support functional and textural properties in order to adjust acidic site density, nature and strength while maintaining open porosity for efficient diffusion of reactants and products.

Acknowledgments

This research was founded by the Conselho Nacional de Desenvolvimento Científico e Tecnológico (CNPq), the Institute of Chemistry of Poitiers: Materials and Natural Resources and the University of Poitiers. Vinicius O.O. Gonçalves is grateful to the Brazilian program Science without Borders. S. Royer acknowledges Chevreul Institute (FR 2638), Ministère de l'Enseignement Supérieur et de la Recherche, Région Nord – Pas de Calais and FEDER.

Appendix A. Supplementary data

Supplementary data associated with this article can be found, in the online version, at <http://dx.doi.org/10.1016/j.apcatb.2017.05.003>.

References

- [1] A. Corma, S. Iborra, A. Velty, Chem. Rev. 107 (2007) 2411–2502.
- [2] T.P. Vispute, H. Zhang, A. Sanna, R. Xiao, G.W. Huber, Science 330 (2010) 1222–1227.
- [3] M. Hara, K. Nakajima, K. Kamata, Sci. Technol. Adv. Mater. (2016).
- [4] J. van Haveren, E.L. Scott, J. Sanders, Biofuels Bioprod. Biorefining 2 (2008) 41–57.
- [5] C. Marcilly, Acidic-Basic Catalysis Application to Refining and Petrochemistry, Technip Ophrys Editions, 2006.
- [6] F. Cherubini, Energy Convers. Manag. 51 (2010) 1412–1421.
- [7] Z. He, X. Wang, Catal. Sustain. Energy 1 (2012) 28–52.

- [8] K. Jacobson, K.C. Maheria, A.K. Dalai, Renew. Sustain. Energy Rev. 23 (2013) 91–106.
- [9] T. Prasomsri, T. Nimmanwudipong, Y. Román-Leshkov, Energy Environ. Sci. 6 (2013) 1732–1738.
- [10] E. Furimsky, Appl. Catal. Gen. 199 (2000) 147–190.
- [11] E.-M. Ryymä, M.L. Honkela, T.-R. Viljava, A.O.I. Krause, Appl. Catal. Gen. 358 (2009) 42–48.
- [12] S. Brilouet, E. Baltag, S. Brunet, F. Richard, Appl. Catal. B Environ. 148–149 (2014) 201–211.
- [13] T. Prasomsri, M. Shetty, K. Murugappan, Y. Román-Leshkov, Energy Environ. Sci. 7 (2014) 2660–2669.
- [14] M. Shetty, K. Murugappan, T. Prasomsri, W.H. Green, Y. Román-Leshkov, J. Catal. 331 (2015) 86–97.
- [15] S. Boullosa-Eiras, R. Lødeng, H. Bergem, M. Stöcker, L. Hannevold, E.A. Blekkan, Catal. Today 223 (2014) 44–53.
- [16] M.W. Nolte, J. Zhang, B.H. Shanks, Green Chem. 18 (2016) 134–138.
- [17] G. Zhou, P.A. Jensen, D.M. Le, N.O. Knudsen, A.D. Jensen, ACS Sustain. Chem. Eng. (2016).
- [18] D. Zhao, J. Feng, Q. Huo, N. Melosh, G.H. Fredrickson, B.F. Chmelka, G.D. Stucky, Science 279 (1998) 548–552.
- [19] C. Ciotonea, B. Dragoi, A. Ungureanu, A. Chiriac, S. Petit, S. Royer, E. Dumitriu, Chem. Commun. 49 (2013) 7665–7667.
- [20] V. Sydorchuk, S. Khalameida, V. Zazhigalov, J. Skubiszewska-Zięba, R. Leboda, K. Wieczorek-Ciurowa, Appl. Surf. Sci. 257 (2010) 446–450.
- [21] N. Bejenaru, C. Lancelot, P. Blanchard, C. Lamonié, L. Rouleau, E. Payen, F. Dumeignil, S. Royer, Chem. Mater. 21 (2009) 522–533.
- [22] B. Dragoi, A. Ungureanu, A. Chiriac, V. Hulea, S. Royer, E. Dumitriu, Catal. Sci. Technol. 3 (2013) 2319–2329.
- [23] A. Ungureanu, B. Dragoi, A. Chiriac, C. Ciotonea, S. Royer, D. Duprez, A. Mamede, E. Dumitriu, ACS Appl. Mater. Interfaces 5 (2013) 3010–3025.
- [24] R.H.R. Castro, D.V. Quach, J. Phys. Chem. C 116 (2012) 24726–24733.
- [25] B.M.Q. Phan, Q.L.M. Ha, N.P. Le, P.T. Ngo, T.H. Nguyen, T.T. Dang, L.H. Nguyen, D.A. Nguyen, L.C. Luu, Catal. Lett. 145 (2015) 662–667.
- [26] F.E. Massoth, Adv. Catal. (1979) 265–310 (H.P. and P.B.W. D.D. Eley, Academic Press).
- [27] J.R. Regalbuto, J.-W. Ha, Catal. Lett. 29 (1994) 189–207.
- [28] S. Rajagopal, H.J. Marini, J.A. Marzari, R. Miranda, J. Catal. 147 (1994) 417–428.
- [29] M.L. Shozai, V.D.B.C. Dasireddy, S. Singh, P. Mohlala, D.J. Morgan, H.B. Friedrich, ACS Sustain. Chem. Eng. 4 (2016) 5752–5760.
- [30] T. Kitano, S. Okazaki, T. Shishido, K. Teramura, T. Tanaka, J. Mol. Catal. Chem. 371 (2013) 21–28.
- [31] R. Radhakrishnan, C. Reed, S.T. Oyama, M. Seman, J.N. Kondo, K. Domen, Y. Ohminami, K. Asakura, J. Phys. Chem. B 105 (2001) 8519–8530.
- [32] E.L. Lee, I.E. Wachs, J. Phys. Chem. C 111 (2007) 14410–14425.
- [33] A. Christodoulakis, E. Heracleous, A.A. Lemonidou, S. Boghosian, J. Catal. 242 (2006) 16–25.
- [34] G. Tsilomelekis, S. Boghosian, Catal. Sci. Technol. 3 (2013) 1869–1888.
- [35] A. Christodoulakis, S. Boghosian, J. Catal. 260 (2008) 178–187.
- [36] V.O.O. Gonçalves, P.M. de Souza, V.T. da Silva, F.B. Noronha, F. Richard, Appl. Catal. B Environ. 205 (2017) 357–367.
- [37] V.O.O. Gonçalves, S. Brunet, F. Richard, Catal. Lett. 146 (2016) 1562–1573.
- [38] E. Furimsky, Catal. Today 217 (2013) 13–56.
- [39] B. Sander, Biomass Bioenergy 12 (1997) 177–183.
- [40] A. Gutierrez, R. Kaila, M. Honkela, R. Slioor, A. Krause, Catal. Today 147 (2009) 239–246.
- [41] C.A. Teles, R.C. Rabelo-Neto, J.R. de Lima, L.V. Mattos, D.E. Resasco, F.B. Noronha, Catal. Lett. 146 (2016) 1848–1857.
- [42] M. Peereboom, B. Van de Graaf, J.M.A. Baas, Recl. Trav. Chim. Pays-Bas 101 (1982) 336–338.
- [43] D.R. Moberg, T.J. Thibodeau, F.G. Amar, B.G. Frederick, J. Phys. Chem. C 114 (2010) 13782–13795.
- [44] Y. Lou, H. Wang, Q. Zhang, Y. Wang, J. Catal. 247 (2007) 245–255.